

BCSJ Award Article**Effect of Hydration on the Very Slow Droplet–Lamellar Transition in Diolelylsulfosuccinate/Decane/Water System: A Small Angle X-ray Scattering Study****Swapan K. Ghosh,^{1,†} Naoki Ichiyanagi,² Hiro-Fumi Okabayashi,^{*2} Aki-Hiro Yoshino,² Takayoshi Takeda,¹ and Charmian J. O'Connor³**¹Faculty of Integrated Arts and Science, Hiroshima University, 1-7-1 Kagamiyama, Higashi-Hiroshima 739-8521²Department of Applied Chemistry, Nagoya Institute of Technology, Gokiso-cho, Showa-ku, Nagoya 466-8555³Department of Chemistry, The University of Auckland, Private Bag 92019, Auckland 1142, New Zealand

Received September 25, 2008; E-mail: fwiw4348@mb.infoweb.ne.jp

Time- and temperature-dependence of the small angle X-ray scattering (SAXS) profiles for homogeneous and transparent solutions of the sodium diolelylsulfosuccinate (SDOleS)–decane–water system with various molar ratios of [H₂O]/[SDOleS] have been examined. The time-dependence of the SAXS profiles has provided evidence that the droplet–lamellar transition occurs spontaneously but very slowly at 298 K. This behavior depends upon the quantity of water solubilized into the SDOleS microemulsions. Some microstructural models have been proposed to explain this very slow transition.

It is well known that dynamic surface phenomena occur in the self-assembled systems formed on the air–water or oil–water interface within the time scale^{1,2} ranging from 10^{−3} to 10³ s. Extensive studies of these phenomena have been carried out for more than seventy years.

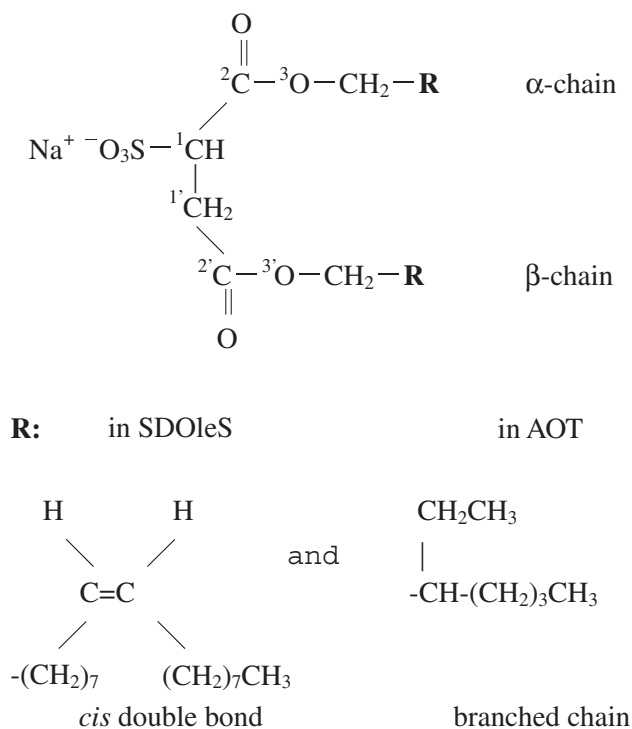
In self-assembled systems of surfactants with low molecular weight, change in surface-tension occurs rapidly (usually in less than 1 s).² Germasheva and Panaeva³ observed a slow surface-tension equilibration in micellar solutions of sulfosuccinates, which could not be interpreted solely on the basis of diffusion to the surface. For very pure samples of sodium diheptylsulfosuccinate (SDHpS), Lucassen and Drew⁴ reported a similar slow surface-tension variation and a simultaneous increase in the surface dilational modulus. They suggested that knowledge of the detailed crystal structure should provide useful information about ordering in a membrane. van den Tempel and Lucassen-Reynders² suggested that slow changes in surface-tension and an increase in elastic modulus might be caused by the cooperative ordering in the surface. The effect of such surface properties on the formation of a three-dimensional (crystalline) structure, similar to that of a lamellar liquid crystal, was studied by Franses et al.⁵ Their results imply that the observed variation in surface-tension is a reflection of the

change in aggregational structure on the surface.

The reversed micelle of sodium 1,2-bis(2-ethylhexyl)sulfosuccinate (AOT) (Scheme 1) incorporates a relatively large number of water molecules in its polar core, thereby forming a water droplet^{6–9} and providing a water/oil interface. In a freshly prepared AOT-reversed micelle, cooperative ordering in the membrane structure at this oil/water interface should occur until the membrane reaches its final ordered state. This concept implies that a difference in the aggregational structure of the interface exists between freshly prepared and aged interfaces. Previous studies on phase behaviors of the AOT–oil–water systems^{7–15} have been focused on the final ordered structures, a limitation imposed by the fast rate of attainment of the final ordered state. However, interpretation of such an ordering process at the molecular level is rare, in spite of the paramount importance of the practical applications of surfactants.

In this present study, an AOT-homolog with longer hydrocarbon chains, sodium diolelylsulfosuccinate (SDOleS) (Scheme 1) has been synthesized. The small angle X-ray scattering (SAXS) technique has then been used to examine the difference in aggregational behavior between the freshly prepared and aged samples for SDOleS–decane–water system. The dynamic molecular models of AOT-reversed micelles^{16–19} and the crystal structures of the AOT-homologs^{4,20} are used to explain the aggregational behavior of the SDOleS–decane–water system at the molecular level.

[†] Present address: Supramolecular Science Laboratory, RIKEN, 2-1 Hirosawa, Wako 351-0198



Scheme 1. Molecular formulae of AOT and SDoleS.

Experimental

Materials. Sodium dioleylsulfosuccinate (SDoleS) was synthesized according to the procedure described in Ref. 16. Maleic acid anhydride was reacted with oleyl alcohol in dried benzene under reflux ($T = 328$ K) for 18 h in the presence of conc. H_2SO_4 . The crude reaction mixture was washed repeatedly with 5 wt % Na_2CO_3 -water solution to remove unreacted maleic acid anhydride and H_2SO_4 , and then dried with anhydrous Na_2CO_3 . Benzene was removed by distillation in vacuum. The dioleyl ester of maleic acid, thus obtained, was identified by $^1\text{H NMR}$ (300 MHz): the chemical shifts (ppm, relative to the internal TMS reference) of ^1H signals in deuterium benzene were 0.8–1.0 for $-\text{CH}_3$, 1.2–1.4 for $-\text{CH}_2-\text{CH}_2-\text{CH}_2-$, 1.5–1.7 for $-\text{O}-\text{CH}_2-\text{CH}_2-$, 1.9–2.1 for $=\text{CH}-\text{CH}_2-$, 3.0–3.3 for $-\text{CH}_2-\text{CO}-$, 4.0–4.4 for $-\text{O}-\text{CH}_2-$ and $-\text{O}_3\text{S}-\text{CH}-$, 5.2–5.4 for $=\text{CH}-\text{CH}_2-$, and 6.2 for $=\text{CHCO}$.

The ester was exhaustively sulfonated in 2-propanol with a three-fold molar amount of 21 wt % NaHSO_3 in H_2O at 373 K (30 h reflux). SDoleS, thus obtained, was recrystallized in methanol and identified by $^1\text{H NMR}$ spectra.

The water content (monohydrate) of the crystalline SDoleS was determined by a Karl-Fisher (MKC-210, Kyoto Electric Ind. Co.) titration.

SAXS Measurements. SAXS was measured with a mirror-monochromator point focusing camera, using the $\text{Cu K}\alpha$ characteristic line from a rotating anode X-ray generator (Rigaku, RU-200) at a power of 50 kV and 150 mA. A one-dimensional position-sensitive proportional counter (MAC science, PSPC-5) was used to measure the scattered beam. The measurable momentum transfer q ($=4\pi/\lambda \sin\theta$, where λ is the wavelength of the incident X-ray beam and 2θ the scattering angle) range was $0.02 \text{ \AA}^{-1} < q < 0.2 \text{ \AA}^{-1}$. The windows of the sample cell were made of capton sheets. The thickness of the samples was approximately

Table 1. Composition of Samples

X^{a}	$W_{\text{f}}^{\text{b}}/\%$	$\Phi_{\text{s}}^{\text{c}}/\%$	$\Phi_{\text{ws}}^{\text{d}}/\%$	$\Phi_{\text{w}}^{\text{e}}/\%$
0	22.7	19.0		0
3.7	21.8	18.7	20.3	1.6
9.5	21.2	18.2	22.2	4.0
20.1	20.0	17.4	25.6	8.1
27.0	19.4	17.0	27.6	10.6

a) Molar ratio: $X = [\text{H}_2\text{O}]/[\text{SDoleS}]$. b) Weight percentage of surfactant: $W_{\text{f}} (\%) = 100W_{\text{s}}/(W_{\text{w}} + W_{\text{o}} + W_{\text{s}})$ (W_{s} , W_{w} , and W_{o} represents weight of surfactant (SDoleS), weight of water, and weight of decane, respectively.). c) Volume percentage of surfactant: $\Phi_{\text{s}} (\%) = 100V_{\text{s}}/(V_{\text{w}} + V_{\text{o}} + V_{\text{s}})$. d) Volume percentage of water + surfactant: $\Phi_{\text{ws}} (\%) = 100(V_{\text{w}} + V_{\text{s}})/(V_{\text{w}} + V_{\text{o}} + V_{\text{s}})$. e) Volume percentage of water: $\Phi_{\text{w}} (\%) = 100V_{\text{w}}/(V_{\text{w}} + V_{\text{o}} + V_{\text{s}})$.

1.5 mm. Sample temperature was changed between 293 and 333 K at intervals of about 5 K, within an accuracy of ± 0.1 K. Observed SAXS intensities were corrected for transmission and background intensities of an empty cell.

Electrical Conductivity Measurement. Electrical conductivity was measured as a function of temperature by a standard impedance meter HiTester 3531Z (Hioki E. Corporation). Two disc electrodes (radius 1.5 mm) were placed 2 mm apart in the sample in a test tube and placed in a temperature-controlled bath. Electrical conductivity was measured at 1 kHz. The sample temperature was measured using a chromel–alumel thermocouple with an accuracy of ± 0.1 K.

Sample Preparation and Determination of Phase Diagram.

The SDoleS (22.7 wt %)–*n*-decane solutions were prepared by weighing SDoleS and *n*-decane into test tubes and equilibrating the mixture in a water bath to the required temperature (± 0.1 K). Five different samples (molar ratio $X = [\text{H}_2\text{O}]/[\text{SDoleS}] = 0, 3.7, 9.5, 20.1, \text{ and } 27.0$) were prepared by adding weighed amounts of water to the SDoleS solutions in ampules which were then sealed, homogenized by heating (323–333 K) and shaken.

The composition of each sample, specified by the water-to-surfactant (SDoleS) molar ratio (X), the weight percentage (W_{s} (%)) and the volume percentage (Φ_{s} (%)) of surfactant are listed in Table 1. When calculating these quantities, the molecular weight and the volume of SDoleS molecule used were 720 g mol^{-1} and $1292 \text{ \AA}^3 \text{ mol}^{-1}$, respectively. The phase feature was determined by visual inspection of the samples in the ampules kept in a water-bath at a controlled temperature (293–333 K). The samples in sealed ampules were then kept at 298 K.

The SAXS measurements of fresh samples were made within three days after preparation of the samples. SAXS measurements were also made on aged samples which had been kept at 298 K for six months, after preparation.

Results and Discussion

The phase diagrams for the SDoleS–decane–water ternary systems were determined by visual inspection at intervals of 5 K in the temperature range 293–333 K. Representative diagrams at 298 and 333 K are shown in Figure 1. Within this temperature range, the phase diagrams consist of three regions (A, B, and C) in general. A homogeneous and transparent one-phase solution was obtained in region A, a homogeneous, transparent, and viscous gel-phase in region B, and a turbid one-phase solution in region C.

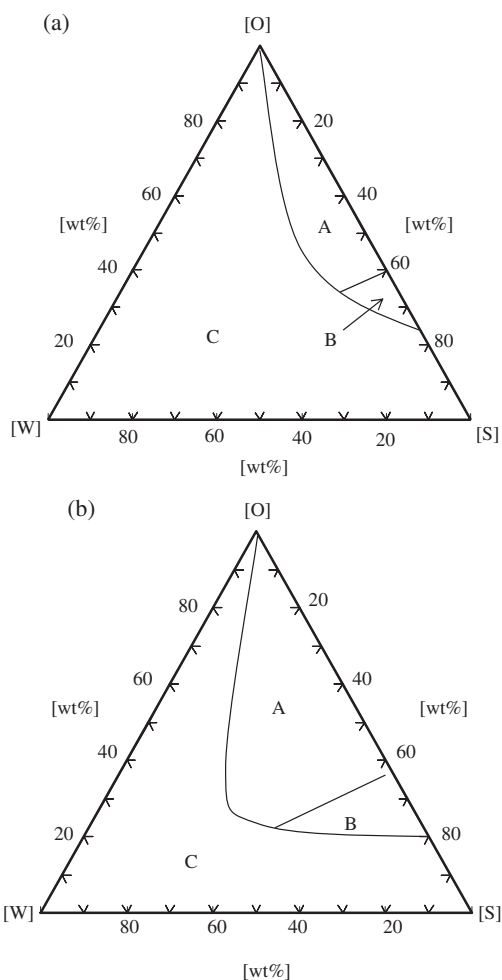


Figure 1. The phase diagrams of SDOleS–decane–water (S–O–W) system for (a) 298 and (b) 333 K. A represents transparent one-phase solution, B represents transparent and viscous gel-phase, and C represents turbid one-phase solution.

For the five samples with four water contents in region A, the volume percentages of water molecules solubilized into the SDOleS–decane system are approximately 1.6–10.6% (Table 1). Therefore, we may assume that water-in-oil type microemulsion (droplet type reversed micelles) forms in the samples and the bicontinuous structure does not exist in these samples.¹

In the present study, both fresh and aged samples of solutions in region A were prepared, in order to be able to examine the difference in aggregational structure of the initial and final states. We assumed that the time taken to reach the final state should depend upon the molar ratio $X = [\text{H}_2\text{O}]/[\text{SDOleS}]$. However, it is very difficult to estimate the time required for each sample to attain equilibrium. We simply speculate that all fresh samples will reach the final ordered state within six months at 298 K if they remain untouched, and may then be examined by SAXS.

The SAXS profiles of the fresh samples for region A are shown in Figure 2. Results reveal that for $X = 0$ sample, SAXS profile does not show any Bragg peak within q range 0.024–

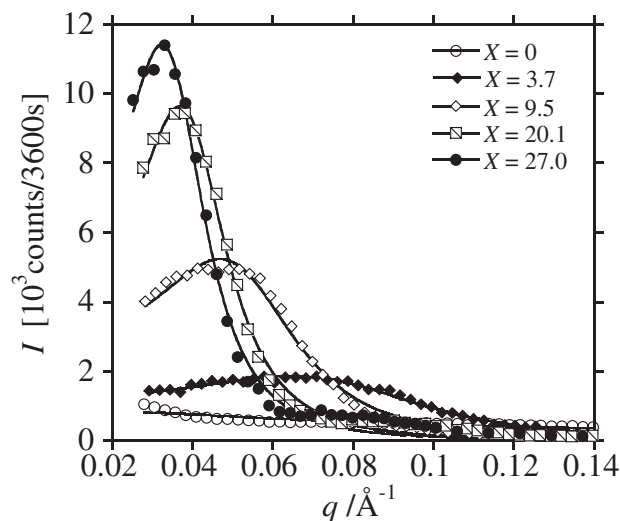


Figure 2. Observed SAXS profiles of the fresh samples (molar ratio $X = [\text{H}_2\text{O}]/[\text{SDOleS}]$) and calculated curves (solid lines) of best fit to the Teubner–Strey model (eq 1).

0.14 \AA^{-1} . This implies that no long-range correlation exists in the dehydrated samples. However, as water molecules are solubilized into SDOleS–decane system, SAXS profiles show distinct scattering peaks with increasing intensities. A broad single Bragg peak at lower q (0.04–0.10 \AA^{-1}) appears for the $X = 3.7$ sample. As X increases, the Bragg peak shifts to lower q ($q = 0.037 \text{\AA}^{-1}$ for $X = 20.1$ and $q = 0.033 \text{\AA}^{-1}$ for $X = 27.0$) and becomes both sharper and much more intense ($I(q)$). These observations indicate that the Bragg peaks arise from the inter-droplet long range correlation in the microemulsions, and depend on the molar ratio X .

To explain these SAXS profiles, we used the scattering function proposed by Teubner–Strey,²¹ which provides the mean displacement between water domains in a mesoscopic scale, and is expressed by eq 1,

$$I(q) = \frac{1}{A + Bq^2 + Cq^4} \quad (1)$$

where $A > 0$, $C > 0$, and $B < 0$. This phenomenological model has been used successfully to determine the structural evolution in both droplet and bicontinuous microemulsion systems.²¹

From the coefficients A , B , and C , such structural parameters as the average repeat distance D between two water or oil domains and the spatial correlation length ξ , as given by eqs 2 and 3, respectively, may be calculated.

$$D = 2\pi \left[\frac{1}{2} \left(\sqrt{\frac{A}{C}} - \frac{B}{2C} \right) \right]^{-\frac{1}{2}} \quad (2)$$

$$\xi = \left[\frac{1}{2} \left(\sqrt{\frac{A}{C}} + \frac{B}{2C} \right) \right]^{-\frac{1}{2}} \quad (3)$$

The parameter $\kappa \equiv 2\pi/D$ provides a dimensionless quantity $1/\kappa\xi$, proportional to the polydispersity of the domain size, which can be regarded as an indicator of a disordered structure.⁸ The data in the SAXS profiles were fitted to eq 1 and thence D and ξ were obtained. The best-fit profiles are

Table 2. Characteristic Scale Length D , ξ , and Disordered Parameter $1/\kappa\xi$, Extracted from the Best Fit to the Teubner–Strey Theory (eq 1) of the Observed Data (298 K), for the Fresh Samples (B: Negative Coefficients in Relative Units and Subscript: 1, Disordered Microemulsion)

X	$D_1/\text{\AA}$	$\xi_1/\text{\AA}$	B	$1/\kappa\xi_1$
3.7	83.20	25.99	-0.13	0.51
9.5	120.48	43.91	-0.15	0.44
20.1	157.81	72.51	-0.24	0.35
27.0	178.30	80.64	-0.25	0.35

also shown in Figure 2 (solid lines) and the values of D_1 , ξ_1 , and $1/\kappa\xi_1$ are listed in Table 2. The parameters D_1 and ξ_1 increase with increasing X , implying that an increase in the amount of solubilized water induces an ordered structure in the ternary system. Since a larger value of $1/\kappa\xi_1$ corresponds to a more disordered structure, a decrease in the value of this parameter implies an increase in the extent of ordering in the system. An increase in X brings about an increasingly ordered structure in the reversed micelles (Table 2), indicating that polydispersity decreases with increasing X .

The hydration number (X) of an AOT molecule is 2–13, depending on the method used for its determination: IR and NMR studies: 2–3^{22a} and 3.5,^{22b} differential scanning calorimetry, ESR spin labelling, and ²H NMR: 2–13,^{22c} and ²H NMR spin–lattice relaxation study: 6.¹⁸ We assume that the hydration number of SDOleS having the same polar groups as AOT is 3–4.

Thus, for the fresh sample with $X = 3.7$, water molecules are probably bound on the polar heads ($\text{SO}_3^- \text{Na}^+$) in the reversed micelles, while for that with $X = 9.5$, water molecules other than bound water may form a very small water pool within a small aggregate in decane. In these microemulsions, SDOleS molecules probably form a small reversed micelle,^{23a,23b} made up of only a few monomers. The broad SAXS profiles of low intensity for these samples suggest the existence of polydispersed small reversed micelles and the absence of any long-range correlations among the reversed micelles.

For the samples with $X = 20.1$ and 27.0, solubilization of excess water into the polar region induces formation of the droplet with a water core, whose domain size depends upon the X value, probably reflecting the SAXS profiles of these fresh samples.

The SAXS profiles of the aged samples are shown in Figure 3. For the sample with $X = 3.7$, we see only a single weak and broad Bragg peak at $q = 0.08\text{--}0.12 \text{ \AA}^{-1}$. This observation implies that the average size of the water-solubilized reversed micelles changes with aging of the sample. The $X = 9.5$ sample shows a broad peak at $q = 0.062 \text{ \AA}^{-1}$ and a sharp, strong peak at $q = 0.082 \text{ \AA}^{-1}$, while the samples with $X = 20.1$ and 27.0 furnish a Bragg peak at $q = 0.063 \text{ \AA}^{-1}$ together with a broad peak at 0.047 \AA^{-1} . These facts indicate that the self-assembly system, responsible for the appearance of the peak at high q , coexists with reversed micelles in these samples. Comparison of these data with those obtained in SAXS studies of the AOT–decane–water systems^{13–15} allows us to assign the Bragg peak at low q to a droplet-type reversed

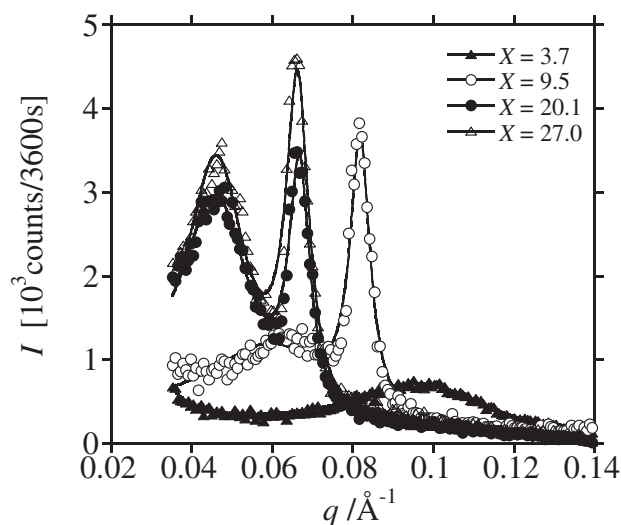


Figure 3. Observed SAXS profiles of the aged samples and calculated curves (solid lines) of best fit to the Teubner–Strey model (eq 4).

micelle and the peak at high q to the first-order peak coming from the stacking structure of a lamellar. The second-order peak was not observed, probably suggesting that there is no long range correlation between fluctuations of the surfactant concentration or the scattering from fluctuation of the surfactant concentration was so small that it was not possible to separate it from the background scattering. A sharp Bragg peak at high q allows calculation of the repeat distance of a lamellar for each sample: assuming a repeat distance (D_1) of $2\pi/q$, $D_1 = 76 \text{ \AA}$ for $X = 9.5$ and $D_1 = 90\text{--}105 \text{ \AA}$ for $X = 20.1$ and 27.0.

The Teubner–Strey model²¹ has also been applied to a comparison of the extent of ordering in the aggregational systems for the aged and fresh samples. It is emphasized that the same theoretical model has been used so as to ensure validity of the comparison.

Teubner and Strey²¹ suggested that their model may explain the ubiquitous appearance of the lamellar phase in the vicinity of the microemulsion. Vonk, Billman, and Kaler²⁴ presented a model in which the microstructure of a bicontinuous microemulsion is taken as that of a distorted lamellar structure with alternating water and oil layers separated by surfactant monolayers. Indeed, the lamellar repeat distance, calculated using this model, is almost exactly equal to the periodicity, D , of the domain size extracted from the Teubner–Strey model.¹⁰ Therefore, when we use the Teubner–Strey model to analyze the Bragg peak arising from a lamellar, the extracted periodicity, D , may be used as an indicator of the repeat distance between the two water or oil domains in a lamellar structure.

The function chosen to fit the SAXS data of aged samples was

$$I(q) = \frac{1}{A + Bq^2 + Cq^4} + \frac{1}{A' + B'q^2 + C'q^4} \quad (4)$$

where $A > 0$, $C > 0$, and $B < 0$, thus providing eqs 2 and 3, and $A' > 0$, $C' > 0$, and $B' < 0$. Figure 3 (solid lines) shows the curves of best fit, and the agreement is excellent. From the

Table 3. D , ξ , and $1/\kappa\xi$, Extracted from the Best Fit to the Teubner–Strey Theory (eq 4) of the Observed Data for the Aged Samples and (b) Their Temperature Dependence (B and B' , Negative Coefficients; Subscripts: 1, Disordered Microemulsion and 2, Lamellar)

X	T/K	$D_1/\text{\AA}$	$\xi_1/\text{\AA}$	B	$1/\kappa\xi_1$	$D_2/\text{\AA}$	$\xi_2/\text{\AA}$	B'	$1/\kappa\xi_2$
3.7	298	63.71	41.07	-1.18	0.247				
	313	61.41	40.53	-1.19	0.241				
	323	59.85	36.94	-1.06	0.258				
	333	58.70	36.09	-1.06	0.259				
9.5	298	101.09	55.24	-1.26	0.291	76.96	329.12	-16.38	0.037
	313	99.00	52.75	-0.90	0.299	75.90	302.14	-13.57	0.040
	323	95.41	45.68	-0.50	0.332	75.33	378.85	-12.80	0.032
	333	88.14	45.26	-0.26	0.310				
20.1	298	134.16	91.96	-1.45	0.232	93.97	307.89	-16.30	0.049
	318	136.40	70.59	-0.84	0.308	94.14	309.03	-13.18	0.049
	328	135.74	64.90	-0.85	0.333	93.69	301.91	-11.70	0.049
	333	138.07	58.32	-0.79	0.377	93.21	308.74	-11.20	0.048
27.0	298	134.26	98.36	-1.52	0.217	94.63	328.54	-13.81	0.046
	318	133.25	90.99	-1.18	0.233	94.36	311.85	-10.16	0.048
	328	132.06	57.17	-0.46	0.368	93.68	357.58	-11.01	0.042
	333	130.31	49.80	-0.35	0.417	93.04	362.27	-10.83	0.041

coefficients A , B , and C , we obtain the average repeat distance D_1 between two water or oil domains, and the correlation length ξ_1 in the droplet structure which leads to detection of the broad peak at lower q . By using eqs 2 and 3, in which the coefficients A , B , and C are replaced by A' , B' , and C' , we obtain the average repeat distance D_2 between two water or oil domains and the correlation length ξ_2 in the lamellar structure. The structural parameters, D_1 , ξ_1 , D_2 , and ξ_2 , and the ordered parameters, $1/\kappa\xi_1$ and $1/\kappa\xi_2$, thus calculated, are listed in Table 3.

For the aged samples at 298 K, the D_1 value in the droplet structure approaches a constant value, ca. 134 Å, with increasing X . Moreover, the parameter $1/\kappa\xi_1$ becomes much smaller than those for the fresh samples, and approaches a constant value, ca. 0.23. This result implies a greater ordering in the droplet structure (the extent of polydispersity becomes smaller). Furthermore, in the lamellar structure, the value of D_2 approaches the constant value of 94–95 Å as X increases.

The $1/\kappa\xi_2$ values, for the aged samples with $X = 20.1$ and 27.0 at 298 K, become much smaller than those in the droplet (Table 3), indicating more extensive ordering in the lamellar state.

Droplet-type reversed micelles with a water core and lamellar structures probably coexist in the aged samples. Accordingly, it is evident that aging the samples for six months had induced the droplet–lamellar (D–L) transition. Moreover, since the Bragg peak arising from a lamellar did not appear for the aged sample with $X = 3.7$, the extent of hydration is critical for this transition. Accordingly, time-dependent variation of hydration in the membrane structure should be related to this slow transition.

The time-scale of a micelle-to-vesicle transition is about 0.1 s and that for a vesicle-to-micelle transition is around 15–90 s.²⁵ These time-scales are in accord with the kinetics of formation of micelles and vesicles.²⁶ Relaxation times of micelles are usually of the order of 10^{-2} – 10^{-9} s, and those of

vesicles are in the range of 0.1 s to a day.²⁶ Therefore, we may now note that the time-scale (between three days and six months) of the D–L transition in the SDOleS–decane–water system (at 298 K) is very much longer than those of a vesicle-to-micelle transition.

For aged samples with $X = 3.7$, 9.5, 20.1, and 27.0, SAXS spectra were also measured at different temperatures in the range 293–343 K. Representative scattering profiles for temperature (T)-dependence of the samples $X = 9.5$ and 27.0 are shown in Figure 4.

For $X = 3.7$, broad peaks arising only from reversed micelles were observed in this T -range (spectra not shown). Furthermore, it was found that an increase in T brought about a decrease in $I(q)$ and a shift of a broad peak (from $q = 0.095 \text{ \AA}^{-1}$ at 298 K to $q = 0.105 \text{ \AA}^{-1}$ at 338–343 K).

For $X = 9.5$, in addition to the weak and broad peak ($q = 0.06$ – 0.07 \AA^{-1}) of reversed micelles, a stronger sharp peak ($q = 0.08 \text{ \AA}^{-1}$) arising from a lamellar was observed. At 293–313 K, the $I(q)$ value of the lamellar peak at high q increases gradually with an increase in T . However, a rapid increase in $I(q)$ occurs at ca. 318 K, and above this temperature $I(q)$ decreases until the sharp peak at high q disappears finally at $T > 333$ K and only the broad droplet peak appears with increasing intensity. This observation implies that the lamellar structure of the $X = 9.5$ sample is unstable at higher temperature.

For $X = 27.0$, $I(q)$ of the lamellar peak at high q increases rapidly within 313–323 K and then becomes almost constant above 333 K. For $X = 20.1$ (spectrum not shown), $I(q)$ also increases with increasing T , but to a lesser extent than with $X = 27.0$. However, for X equal to both 20.1 and 27.0, the intensity of the broad droplet peak at low q decreases above 333 K. These trends in $I(q)_{\text{max}}$ for the droplet and lamellar peaks, observed with increasing T , are consistent with occurrence of a first-order transition from a droplet to a lamellar structure.

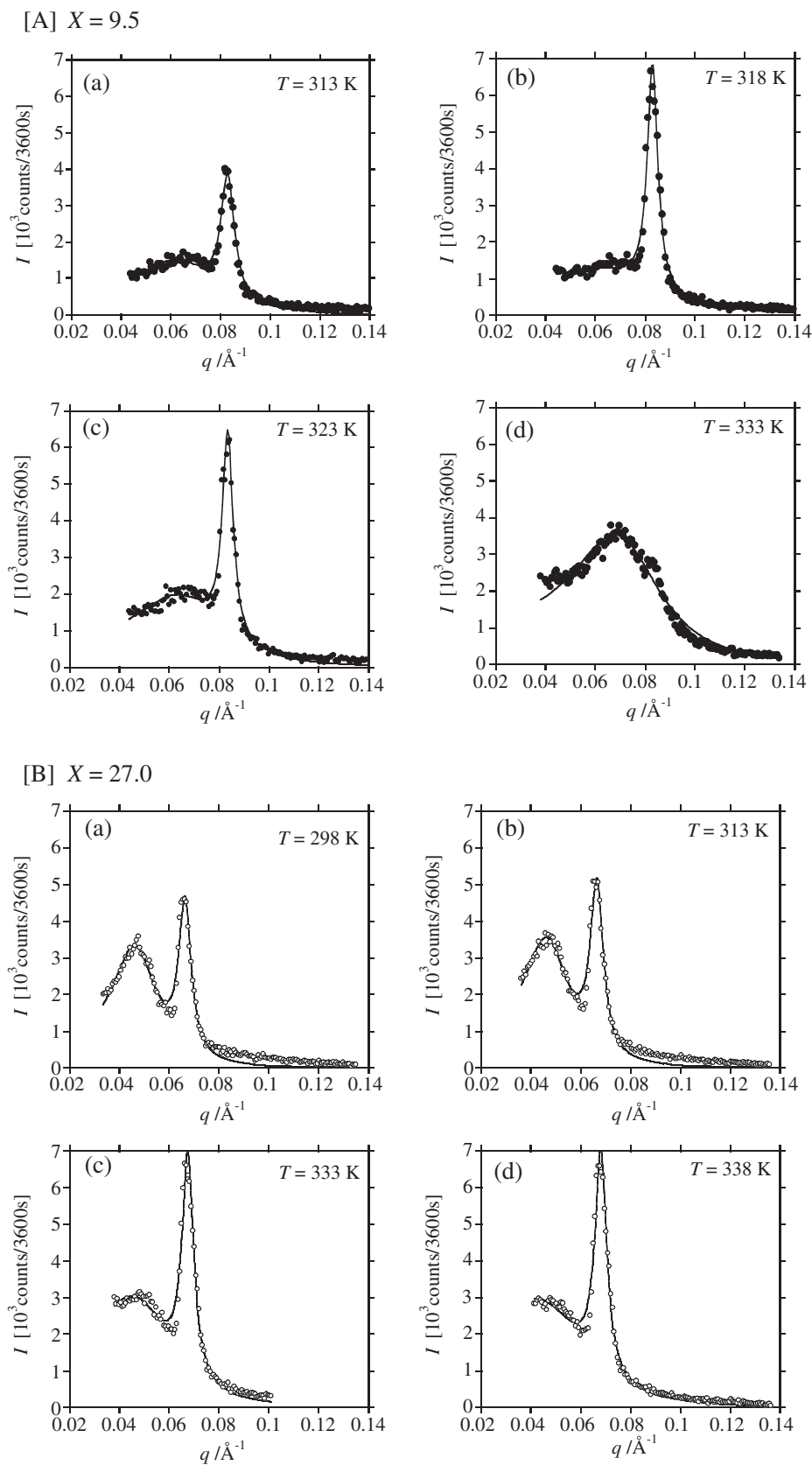


Figure 4. Representative T -dependence of SAXS profiles for the aged samples ([A]: $X = 9.5$: (a) 313, (b) 318, (c) 323, and (d) 333 K and [B] $X = 27.0$: (a) 298, (b) 313, (c) 333, and (d) 338 K) and calculated curves (solid lines) of best fit to the Teubner–Strey model (eq 4).

Such a temperature dependence of the lamellar peaks for $X = 20.1$ and 27.0 indicates that the lamellar structure of these samples is relatively stable at higher temperature. That is, the stability of a lamellar for the SDOleS–decane–water system strongly depends upon the quantity of water solubilized into the polar region. This observation may reflect the extent of the hydrogen-bonding network formed among the polar groups.

These T -dependent SAXS spectra were fitted using eq 4. Representative best fits to the observed data are shown in Figure 4 (solid lines). The T -dependence of the extracted parameters is also listed in Table 3. It is evident that a rise in T brings about a decrease in D_1 for a droplet for all the samples. The parameter $1/\kappa\xi_1$, an indicator of disordering, tends to increase with a rise in T . In particular, for $X = 27.0$, a rapid increase in $1/\kappa\xi_1$ occurs above 318 K. Since the magnitude of $1/\kappa\xi_1$ is proportional to the polydispersity of a domain size, we may assume that a rise in T brings about an increase in the extent of polydispersity of the droplet structure. Thus, these results may be ascribed to a increase in the extent of disordering of the droplet structure with increasing T .

The repeat distance, $D_2 = 2\pi/q_0$, of a lamellar structure, for the aged samples at higher X , changes little with increasing T . This trend differs from that seen with D_1 in the droplet, a consequence of the greater ordering in a lamellar, even at higher temperature, indicating formation of a very stable lamellar. In fact, the values of $1/\kappa\xi_2$ are much smaller than $1/\kappa\xi_1$ in a droplet and their T -dependence is very small.

Thus, the T -dependence of the SAXS profiles for the aged samples depends definitely upon the X -value, reflecting a structural change of the self-assembly.

At higher temperature, lysis of droplet structures may occur.^{18,23a,23b} For the $X = 3.7$ sample, rather than postulating the usual reversed micelles, we must postulate the presence of smaller oligomers or micellar fragments,^{23a,23b} which may be dispersed in the non-polar solvent as water-solubilized small aggregates. We speculate that SDOleS molecules, constituting a small aggregate, are linked through an intermolecular hydrogen-bonded network in the small polar cavity. However, in the $X = 3.7$ sample, the amount of water solubilized in the polar cavity may be too small to allow formation of a dense-droplet. Furthermore, a rise in T may result in further lysis and reduction in the size of the small aggregates. This reduction may be reflected in the SAXS spectral features of the aged sample with $X = 3.7$ at higher T .

To explain the T -dependent SAXS behavior of the aged sample with $X = 9.5$, we may consider the role of fusion among lamellar fragments or small aggregates. As T increases, such small lamellar fragments get bigger after fusion through collisions, bringing about formation of a lamellar with D_2 value equal to ca. 77 \AA . A further rise in T above 333 K causes probable lysis of the lamellar, leading finally to disappearance of the lamellar peak at higher T (343 K). The origin of this lysis is probably due to the amount of solubilized water that may be insufficient to form a stable lamellar. The lamellar peak at $q = 0.082 \text{ \AA}^{-1}$ may originate from formation of an unstable lamellar fragment with a small hydrogen-bonding network.

The increase in $I(q)$ within the temperature range of 333–343 K, for the lamellar peaks of samples $X = 20.1$ and 27.0 , indicates that these lamellar become more stable at higher T and

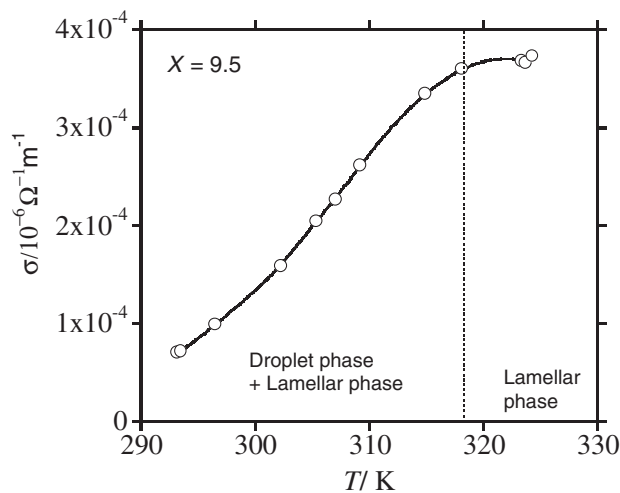
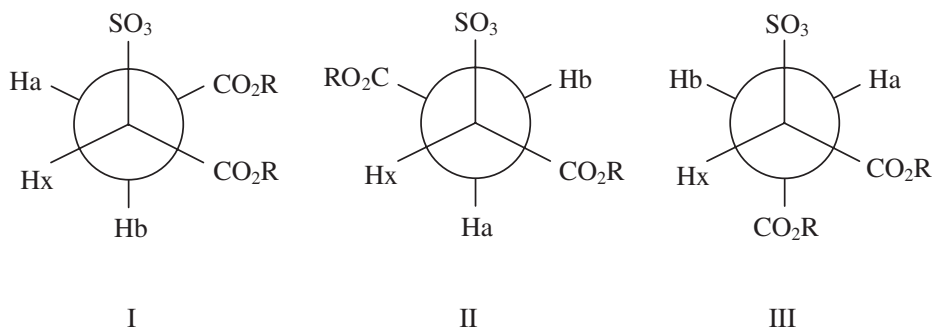


Figure 5. Electrical conductivity, σ is plotted as a function of T . The change in the slope of the conductivity curve around 318 K indicates a droplet–lamellar transition.

are much more stable than that for $X = 9.5$. As the amount of water in the polar core increases, the network of hydrogen bonds may spread further along the ester regions to prevent lysis of the lamellar, resulting in stabilization of the lamellar at higher T .

In order to elucidate the temperature dependencies of the structural evolution of aggregates, we measured electrical conductivity (σ) for $X = 9.5$ as a function of temperature within the temperature range 293–324 K. Results show that with increasing temperature σ increases monotonously and finally saturates at around 318 K (Figure 5). In the sample with relatively small surfactant volume, we may account for the increase in electrical conductivity by considering the mobility of positively and negatively charged water droplets under the applied electric field.^{27,28} The charge fluctuations of a water nano-droplet occur due to exchange of surfactant anions with the surrounding pool of surfactant monomers.^{29,30} When a surfactant anion departs a reversed micelle (or small reversed micelles), it leaves behind a counter ion in the water core. Thus, the micelle will carry a single positive charge. When a surfactant anion from the bulk phase is incorporated within a reverse micelle, the droplet will become negatively charged by one unit. Results suggest that the structural modification, that occurs at around 318 K, can be accounted for by invoking a transition from a reversed micellar structure (a hydrocarbon continuum) to a lamellar phase (a water continuum) whose conductivity remains almost constant. Measurement of electrical conductivity at $T > 324 \text{ K}$ was unsuccessful because a white precipitate was found, supporting the occurrence of lysis of the lamellar structures.

In the Chen et al.¹⁰ investigation of the T -induced D–L transition for the AOT–oil–water system, an increase in T accelerated dissociation of the counter ion of an AOT molecule, making electrostatic repulsion among the head groups more intense. It was therefore proposed that spontaneous curvature of the AOT-reversed micelle became smaller and then the droplet structure was destabilized, inducing the D–L transition.



Scheme 2. Possible rotational isomers about the $^1\text{CH}-^1\text{CH}_2$ single bond of the succinate segment.

This mechanism may be applied to the D–L transition of the present SDOleS system, since we find that an increase in the amount of solubilized-water accelerates dissociation of the counter ion, increasing electrostatic repulsion among the head groups.

Nagao et al.¹³ noted that the pressure-dependent small-angle neutron scattering profiles of the AOT–oil–water system reflect the D–L transition caused by a change in interactions between the hydrophobic groups and oil. In the pressure-dependent SAXS studies of the same system, Seto et al.^{14,15} concluded that the hydrophobic interaction becomes more intense with increasing pressure, leading to the D–L transition.

Since the origin of such transitions for the AOT–oil–water systems still remains unresolved at the molecular level, elucidation of the relationship between hydration (hydrogen bonds) and the membrane structures is highly desirable.

We are now able to interpret the present D–L transition of the SDOleS systems at a molecular level, using the experimental results thus far obtained for both AOT and its homologs (sodium dialkylsulfosuccinates (DAS)).^{16–20,31} Results of special relevance to this present study may be summarized as follows.

(1) An AOT or DAS anion has three sites (SO_3^- and two O–C=O groups) for hydration. When the amount of water incorporated into the reversed DAS micelles is small, water molecules may be bound predominantly first to the $\text{SO}_3^- \text{Na}^+$ head groups, thereby causing strong hydrogen-bonding networks among the head groups.^{17,18} With an increase in water-content, further incorporation of water molecules into the ester regions may occur, according to the fjord and reef models of hydration.³² Thus, weak intra- or intermolecular hydrogen-bonding networks may be further formed between neighboring ester groups in the aggregates.^{17,18}

(2) If we assume that the three rotational isomers I, II, and III (Scheme 2) of an AOT anion represent the minimum energy staggered conformations for rotation about the $^1\text{CH}-^1\text{CH}_2$ single bond (Scheme 1), we may calculate the fractional populations (P_I , P_{II} , and P_{III}) of the three rotational isomers from the NMR coupling constants (J_{ax} and J_{bx}) for the $^1\text{CH}-^1\text{CH}_2$ protons. In our previous paper,¹⁸ the P_I , P_{II} , and P_{III} values were calculated using the J_{ax} and J_{bx} values measured at various $[\text{D}_2\text{O}]/[\text{AOT}]$ molar ratios (R) for the AOT– C_6D_6 – D_2O system. The results indicated that the fractional population P_{III} of type III increases with an increase in R , while the P_I and P_{II} values of types I and II tend to decrease, indicating

that an increase in R induces stabilization of type III in this system. Furthermore, it has been found that the rise in temperature results in an increase in P_{II} , implying the extension of two AOT–hydrocarbon chains into the apolar solvent phase (Thus, this conformation (type II) may be regarded as an open type I).

(3) A single-crystal X-ray structural analysis of DAS⁴ with longer chains provides evidence that type III is preferentially stabilized, bringing about the conformation with close mutual contact between the two DAS–hydrocarbon chains (in this sense we denote type III as a closed type I).

(4) In addition to the conformations about the $^1\text{CH}-^1\text{CH}_2$ single bond, the difference in the torsion angle of the $^1\text{C}-^1\text{C}-^2\text{C}-^3\text{O}$ segment also induces the open type II or closed type II.^{4,20,31}

(5) ^1H and ^{13}C NMR studies¹⁹ of the AOT– C_6D_6 – D_2O system in reversed micelles, assisted by 2-D nuclear Overhauser effect and the rotating-frame Overhauser enhancement and ^{13}C NMR T_1 methods, provide the detailed dynamic models of open and closed types.

Thus, in an AOT or DAS anion, molecular conformations of both open and closed types, in addition to other conformations, are possible (Figures 6Aa and 6Ab), and the inter-conversion among them probably occurs in the aggregates. However, we may assume that the open-type conformations are preferentially stabilized in the aggregates (Figure 6B), based on the experimental results mentioned above. An open type makes it possible to form a droplet while a closed type makes for easy provision of a lamellar.

A molecular structural model, which may be associated with the mechanism of the present D–L transition, is now presented.

In the fresh samples ($X = 20.1$ and 27.0) forming droplets or the fresh $X = 9.5$ sample providing small reversed micelles, an open type is probably stabilized initially, although the other conformations also coexist, and the two oleyl chains may fan out randomly in the oil phase (the two ester linkages are in the oil phase and only the $\text{SO}_3^- \text{Na}^+$ groups penetrate into the water core or pool) (Figure 6C). With time, penetration of water molecules into the ester-linkages region of the reversed micelle may occur, inducing cooperative stabilization of the closed type. As a consequence, exclusion of the solvent (decane) may occur. This process may lead to stabilization of a lamellar and consequently to increased hydrophobic interactions between the two oleyl chains. That is, extension of the hydrogen-bonding network accompanied by an increase in water-quantity

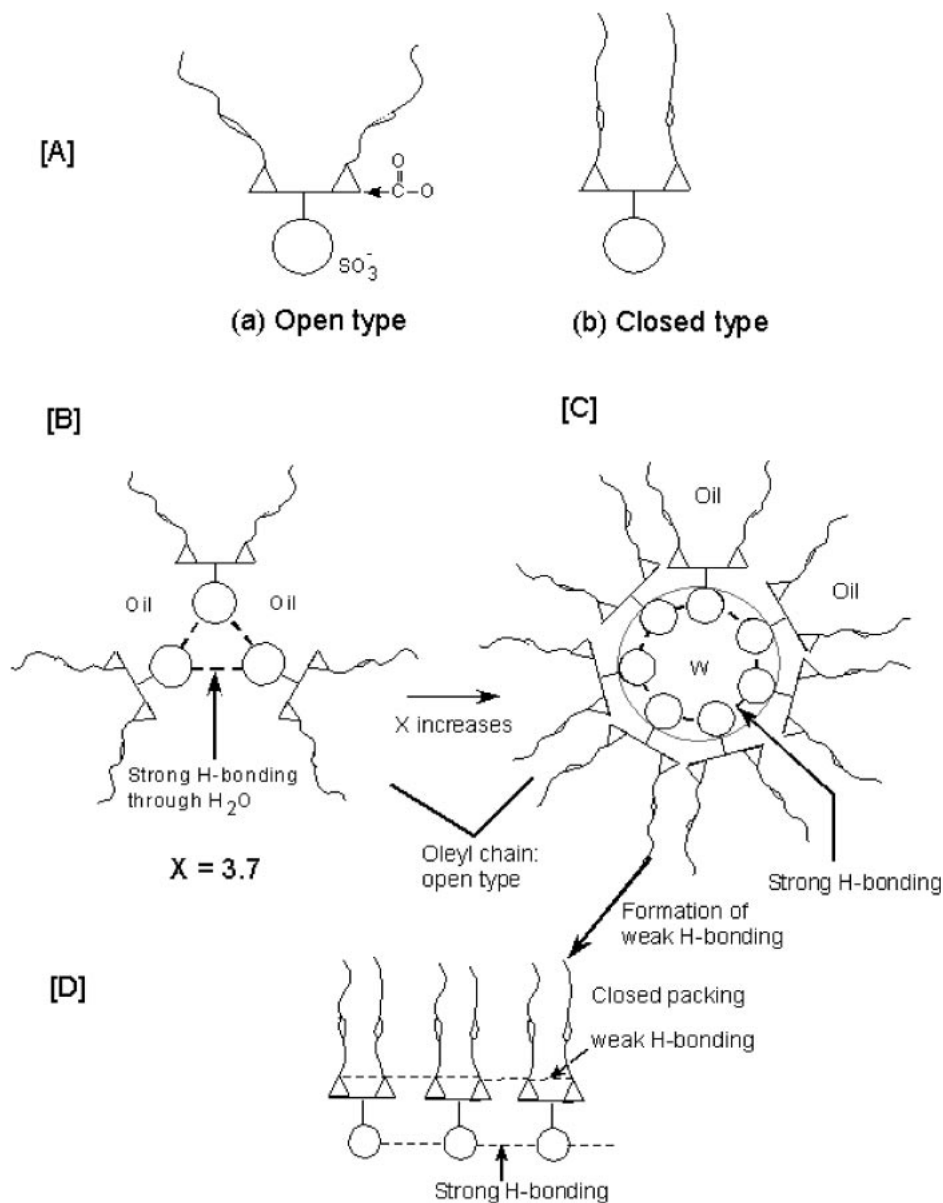


Figure 6. Schematic models for change of [A]: two types of SDOleS, each with three sites for hydration; [B] and [C]: a reversed micelle for a fresh sample with $X = 3.7$ and $9.5\text{--}27.0$, respectively; and [D]: a lamellar showing weak and strong intra- and intermolecular H-bonding networks.

may induce stabilization of the closed type. With an increase in X , very slow penetration of water into the two ester regions (oriented either as a fjord or reef) probably occurs at lower temperatures. Consequently, formation of weak hydrogen-bonding networks among the ester groups and water molecules occurs with an increase in solubilized-water, thereby promoting stabilization of a lamellar structure (Figure 6D).

However, in the $X = 3.7$ sample, stabilization of a closed type to induce stacking of the hydrocarbon chains among neighboring molecules probably does not occur. The reason may be that the ester groups in small reversed micelles are not sufficiently hydrated, since hydration when X is small is localized mainly on the $\text{SO}_3^- \text{Na}^+$ head group, leading to absence of any transition from an open to a closed type configurations.

We therefore suggest that it is the very slow hydration of the ester groups which brings about the conformational change from the open type to the closed type, leading to stabilization of a lamellar. This conformational change model also explains successfully the results of the pressure- and temperature-dependent SANS and SAXS analyses of the AOT–decane–water system, as demonstrated by Nagao et al.¹³ and Seto et al.^{14,15} Their results indicated that a rise in pressure and temperature induces the D–L transition, although this transition does not occur at ambient pressure and ambient temperature. We may attempt to explain this behavior at a molecular level as follows.

In the droplet of the AOT–decane–water system, which is stabilized at ambient pressure and ambient temperature, the open types may be preferentially stabilized. This stabilization

may probably be caused by the steric hindrance of the 2-ethyl group portions of an AOT molecule, which may disturb stacking of the two hydrocarbon chains to form a lamellar. The solvent decane molecules probably penetrate into the grooves of the hydrocarbon chains fanning out into the apolar solvents. A rise in pressure or temperature may induce further penetration of water molecules from the water pool side into the ester-linkage side of a reverse micelle, resulting in the extension of the hydrogen-bonding network to the ester-linkages. Such a transfer of water molecules may cause preferential stabilization of the closed types making it easier to form a lamellar. In the pressure-dependent data shown by Seto et al.,¹⁵ the rise of pressure obviously induces reduction of the water-core radius in the droplet. This observation can be successfully explained by invoking transfer of water molecules from the water pool side to the inner side.

When the conformational change from an open type to a closed type occurs, the exclusion volume (v_s) of a SDOleS molecule becomes smaller, resulting in reduction of the so-called packing parameter³³ ($P_p = v_s/(a_H l_c)$, where v_s , a_H , and l_c are effective molecular volume, effective water contact area per molecule, and effective molecular length, respectively), which causes stabilization of a lamellar.

The hardness of a closed type lamellar may be greater than that of the droplet in which open types are predominant, since the open type SDOleS molecules are able to contain much larger quantities of the solvent, compared with the closed types. Indeed, for the AOT–decane–water system, results of the pressure-dependent Neutron Spin Echo experiments¹³ provided evidence that the hardness of a lamellar induced under high pressure is greater than that of a droplet.

Martin and Magid³⁴ suggested that addition of water to a dried AOT reversed micelle in benzene may induce a conformational change of AOT, resulting in formation of its open extended structure.

For sodium diheptylsulfosuccinate (SDHpS),⁴ it has been confirmed that the extent of hydration affects the nature of the packing of their hydrocarbon chains and the stability of a bilayer structure. The Raman spectra of a series of DAS³⁵ provided evidence that monohydration causes the segment close to the CH₃-terminal to become disordered, although dihydration induces an extended structure of the *n*-alkyl chains. We emphasize that stability of a lamellar arises not only from hydrogen-bonded links in the monolayer plane but also from hydrogen-bonded links between adjacent monolayers.

Lucassen and Drew⁴ presented a model, that allowed formation of alternate optical (S and R) pairs to occur cooperatively on the surface, to explain the observation of a slow surface-tension equilibration for a micellar solution of SDHpS. This concept may be applied to the water-in-oil interface in the SDOleS microemulsion system. Such a cooperative character and the necessity for ordering of the oleyl chains with a cis type double bond may be strong contributors to the slow rate of the present D–L transition at 298 K.

Conclusion

Time- and temperature-dependent SAXS profiles have been analyzed to identify the occurrence of a D–L transition. In the

SDOleS–decane–water system, it has been found that this transition occurs very slowly at 298 K. The extent of this transition depends on the extent of hydration, with formation of a stable lamellar at higher molar ratio of [H₂O]/[SDOleS]. A rise in temperature also promotes the D–L transition. In particular, the hydration effect plays a critical role in ensuring stability of the lamellar and this effect has been successfully explained at the molecular level, using evidence available from previous studies.

References

- 1 B. Jönson, B. Lindman, K. Holmberg, B. Kronberg, *Surfactants and Polymers in Aqueous Solution*, John Wiley & Sons, New York, **1998**, Chap. 12, pp. 247–264.
- 2 M. van den Tempel, E. H. Lucassen-Reynders, *Adv. Colloid Interface Sci.* **1983**, *18*, 281.
- 3 I. I. Germasheva, S. A. Panaeva, *Kolloidn. Zh.* **1982**, *44*, 661.
- 4 J. Lucassen, M. G. B. Drew, *J. Chem. Soc. Faraday Trans. 1* **1987**, *83*, 3093.
- 5 E. I. Franses, J. E. Puig, Y. Talmon, W. G. Miller, L. E. Scriven, H. T. Devis, *J. Phys. Chem.* **1980**, *84*, 1547.
- 6 P. Ekwall, L. Mandell, K. Fontell, *J. Colloid Interface Sci.* **1970**, *33*, 215.
- 7 M. Wong, J. K. Thomas, M. Grätzel, *J. Am. Chem. Soc.* **1976**, *98*, 2391.
- 8 M. Kotlarchyk, S.-H. Chen, J. S. Huang, M. W. Kim, *Phys. Rev. Lett.* **1984**, *53*, 941.
- 9 E. Y. Sheu, S.-H. Chen, J. S. Huang, J. C. Sung, *Phys. Rev. A* **1989**, *39*, 5867.
- 10 S.-H. Chen, S.-L. Chang, R. Strey, *J. Chem. Phys.* **1990**, *93*, 1907.
- 11 J. Eastoe, B. H. Robinson, D. C. Steytler, *J. Chem. Soc., Faraday Trans.* **1990**, *86*, 511.
- 12 J. Eastoe, W. K. Young, B. H. Robinson, D. C. Steytler, *J. Chem. Soc., Faraday Trans.* **1990**, *86*, 2883.
- 13 M. Nagao, H. Seto, T. Takeda, Y. Kawabata, *J. Chem. Phys.* **2001**, *115*, 10036.
- 14 H. Seto, D. Okuhara, Y. Kawabata, T. Takeda, M. Nagao, J. Suzuki, H. Kamikubo, Y. Amemiya, *J. Chem. Phys.* **2000**, *112*, 10608.
- 15 H. Seto, M. Nagao, Y. Kawabata, T. Takeda, *J. Chem. Phys.* **2001**, *115*, 9496.
- 16 A. Yoshino, N. Sugiyama, H. Okabayashi, K. Taga, T. Yoshida, O. Kamo, *Colloids Surf.* **1992**, *67*, 67.
- 17 A. Yoshino, H. Okabayashi, T. Yoshida, *J. Phys. Chem.* **1994**, *98*, 7036.
- 18 A. Yoshino, H. Okabayashi, T. Uchida, T. Ogasawara, T. Yoshida, C. J. O'Connor, *J. Phys. Chem.* **1996**, *100*, 8418.
- 19 A. Yoshino, H. Okabayashi, T. Yoshida, K. Kushida, *J. Phys. Chem.* **1996**, *100*, 9592.
- 20 Y. Nagasoe, N. Hattori, H. Masuda, H. Okabayashi, C. J. O'Connor, *J. Mol. Struct.* **1998**, *449*, 61.
- 21 M. Teubner, R. Strey, *J. Chem. Phys.* **1987**, *87*, 3195.
- 22 a) M. Bey Temsamani, M. Maeck, I. El Hassani, H. D. Hurwitz, *J. Phys. Chem. B* **1998**, *102*, 3335. b) P. Amico, M. D'Angelo, G. Onori, A. Santucci, *Nuovo Cimento Soc. Ital. Fis., D* **1995**, *17*, 1053. c) H. Hauser, G. Haering, A. Pande, P. L. Luisi, *J. Phys. Chem.* **1989**, *93*, 7869.
- 23 a) C. J. O'Connor, T. D. Lomax, *J. Colloid Interface Sci.* **1983**, *95*, 204. b) F. Y. F. Lo, B. M. Escott, E. J. Fendler, E. T.

Adams, Jr., R. D. Larsen, P. W. Smith, *J. Phys. Chem.* **1975**, *79*, 2609.

24 C. G. Vonk, J. F. Billman, E. W. Kaler, *J. Chem. Phys.* **1988**, *88*, 3970.

25 Y. Zheng, Z. Lin, J. L. Zakin, Y. Talmon, H. T. Davis, L. E. Scriven, *J. Phys. Chem. B* **2000**, *104*, 5263.

26 *Surfactant Solutions—New Methods of Investigations: Surfactant Science Series*, ed. by R. Zana, Marcel Dekker, New York, **1987**, Chap. 8, pp. 405–444.

27 H. F. Eicke, M. Borkovec, B. Das-Gupta, *J. Phys. Chem.* **1989**, *93*, 314.

28 D. G. Hall, *J. Phys. Chem.* **1990**, *94*, 429.

29 C. Cametti, P. Codastefano, P. Tartaglia, J. Rouch, S. H. Chen, *Phys. Rev. Lett.* **1990**, *64*, 1461.

30 C. Cametti, P. Codastefano, P. Tartaglia, S.-H. Chen, J. Rouch, in *Structure and Dynamics of Strongly Interacting Colloids and Supra-molecular Aggregates in Solution*, ed. by S.-H. Chen, Kluwer Academic Publishers, **1992**, pp. 807–814.

31 Y. Nagasoe, N. Ichianagi, H. Okabayashi, S. Nave, J. Eastoe, C. J. O'Connor, *Phys. Chem. Chem. Phys.* **1999**, *1*, 4395.

32 F. M. Menger, J. M. Ierkunica, J. C. Johnston, *J. Am. Chem. Soc.* **1978**, *100*, 676.

33 J. N. Israelachvili, in *Intermolecular and Surface Forces Second Edition*, Academic Press, New York, **1992**, p. 369.

34 C. A. Martin, L. J. Magid, *J. Phys. Chem.* **1981**, *85*, 3938.

35 Y. Nagasoe, N. Ichianagi, H. Okabayashi, S. Nave, J. Eastoe, C. J. O'Connor, *Colloid Polym. Sci.* **1999**, *277*, 947.